Cooling silicon photovoltaic cells using finned heat sinks and the effect of inclination angle

Ellis Johnston[1], Peter S. B. Szabo[1, 2], Nick S. Bennett[1, 3]

[1] School of Engineering and Physical Sciences, Heriot Watt University, Edinburgh EH14 4AS, United Kingdom

[2] Bandenburg University of Technology, Cottbus-Senftenberg, Siemens-Halske-Ring 14, D-03046 Cottbus, Germany

[3] Centre for Advanced Manufacturing, Faculty of Engineering and Information Technology, University of Technology Sydney,
PO Box 123, Broadway, NSW 2007, Australia

Nicholas.bennett@uts.edu.au

Abstract This study investigates the reduction in temperature within a silicon solar module by increasing the heat transfer coefficient of its rear surface. Specifically, a combined simulation and experimental study is carried out to determine how the performance of a heat sink mounted on the rear of a module is dependent on orientation, and how fin height influences the heat sink's ability to reduce temperature. With a heat sink fin height of 20 mm, the temperatures of the front and rear surfaces of the module reached 62°C and 51°C, respectively. When the fins are extended to 300 mm, these temperatures reduced to 45°C and 30°C, respectively. It is shown that the heat sink's performance in removing heat decreases when the orientation is rotated through 180° (from facing upwards to facing downwards). The accompanying effect on the power output is also investigated. When the 20 mm heat sink is applied to a solar module, the power output increased by 11.3% (relative), compared to the power generated from a bare solar module. Similarly, the application of a 100 mm heat sink resulted in an increase in power output of 15.3% (relative).

I. INTRODUCTION

Advances in technology, along with a reduction in cost and government policies, have contributed to an increase in photovoltaic (PV) installation across the globe. This being said, PV panels are known for having low conversion efficiency compared to more traditional forms of electricity generation, with the average solar cell having an efficiency of around 15% [1]. Even then, the efficiency of a solar cell is usually tested under standard test conditions (STC), with an irradiance of 1000 W/m^2 and a set temperature of 25 ℃ [2]. Unfortunately, under true operating conditions, the temperature does not remain constant. Typically, silicon solar cells can operate in locations where the ambient temperature can exceed 50 ℃, leading to a 12% reduction (relative) in power output [3].

Many studies have been carried out on the effects of temperature on silicon solar cell performance and it is widely accepted that an increase in temperature negatively affects the power output [4-7]. Relatively speaking, for every degree of temperature increase, the efficiency decreases by up to 0.5% [8]. This is referred to as the temperature coefficient, the lower the value the better the solar cell performs when there is a temperature change. A further issue arises because subjecting a solar cell to continuous high temperatures will accelerate cell degradation [9-10]. This can result in an overall decrease in energy production from a solar module, due to a shorter operational life. Likewise, a future breakthrough in high-efficiency modules (30%) is predicted to be the lead halide perovskite-crystalline silicon tandem cell. Presently, perovskites are sensitive to heat, even under ambient conditions. Thus operating temperature is likely to be a major, if not the most important, hurdle facing their commercial deployment [11]. Therefore, methods to reduce a module's operating temperature have been researched. There are two methods that can be employed to reduce the temperature within a module – either aiming to reduce the production of heat, or improve the rejection of waste heat [12].

A. Altering Physical Properties

To date there are a range of techniques that have been investigated to reduce the temperature of solar modules. Some studies consider the change of physical properties of the solar module, e.g. the thermal conductivity of the backsheet or encapsulant. However, those studies only report modest reductions in temperature of, for example, 1 ℃ [3, 12]. Replacing the standard tedlar backsheet with a glass backsheet resulted in a slight increase in temperature [3, 13]. Reasons for this are that although the glass had a higher thermal conductivity than tedlar, the thickness of a glass sheet is larger than that of a standard tedlar sheet. As part of this current study a simulation is carried out that validates these findings and is discussed in Section 3.

B. Active Cooling Techniques

Active cooling mechanisms can reduce the temperature of the solar cell e.g. by using forced convection. A common active cooling technique extracts heat from the solar cell using pumps to transport water through the equipment. This technique has a large cooling capacity for solar cells [14, 15]. When hybrid solar cells are used to heat water in addition to their photovoltaic function, the cells temperature can reduce by up to 16 ℃, increasing the systems overall efficiency by 57 % [14]. Similar to water, air cooling could potentially decrease the solar cells temperature but was found to be less effective and resulted in reductions of only 2 ℃ to 5 ℃ [16-18]. A recent novel active cooling technique explored in reference [19] suggested evaporative cooling. This technique is based on droplets of water sprayed onto a porous material to cool PV cells.

C. Passive Cooling Techniques

60   Passive cooling techniques require no additional energy input, instead they enhance heat transport by natural convection to cool

61   the solar cell [20]. Using phase-change materials (PCMs) to cool solar cells is another passive approach. Stropnik and Stritih

62   determined that PCMs can reduce the temperature by 35.6 ºC [21]. Huang et al. also obtained large temperature reductions using

63   PCMs [22]. A further passive cooling technique which has been investigated is the addition of heat sinks, or fins, to the rear side

64   of the cell. Research undertaken previously has indicated that heat sinks are a suitable affordable passive cooling technique. For

65   example, a study carried out by Cuce [20] explores this. For an ambient temperature of 35 ºC, a temperature reduction was recorded

66   of 12.2 ºC. It was found that as the ambient temperature increased, the temperature reduction within the solar cell with a heat sink

67   increased. Amr et al. [23] investigates a heat sink's performance in both still air and ventilated air (1 m/s), as well as looking at the

68   effect of heat sink material, thickness, spacing and height. It was noted that the panel with fins had an average electrical efficiency

69   of 13.9%, which was 1.8% higher than the module without fins (12.1%). Natarajan et al. [24] studied the application of heat sinks

70   to a photovoltaic concentrator system. The effects of varying fin thickness and height were measured, resulting in a

71   recommendation for a heat sink containing 4 fins of 1 mm thickness and a height of 5 mm. Increasing fin thickness did not yield a

72   significant temperature change; however, a change in height from 2.5 mm to 5 mm decreased the cell temperature by 4.3 ºC and a

73   further change to 20 mm resulted in an additional 10 ºC temperature reduction.

74   In addition to the fin/heat sink geometrical design, one would expect its overall cooling effectiveness to be dependent on

75   orientation. Here we define orientation as the inclination angle, based on a heat sink being mounted to the backside of a solar

76   module, which might be mounted horizontally or on some incline, e.g. to match the angle of a roof. Indeed Xu et al. [25]

77   investigated the temperature of cells as a function of inclination angle and found differences of around 15 ºC for inclines between

78   0 º (horizontal) and 60 º. This study focused only on the case of concentrated PV. In this current work we investigate this inclination

79   dependence for the case of standard silicon PV cells using a complimentary numerical and experimental study.

80

II. ALTERING SOLAR MODULE ARCHITECTURE

82   Initially, the effect of altering the physical structure and thermal properties of a solar module on the module temperature is

83   investigated. A MATLAB script derived from Allan, Pinder and Dehouche [26], is employed. The script can calculate the

84   temperatures in each layer of the solar module. The structure of a standard solar module is displayed in Figure 1.
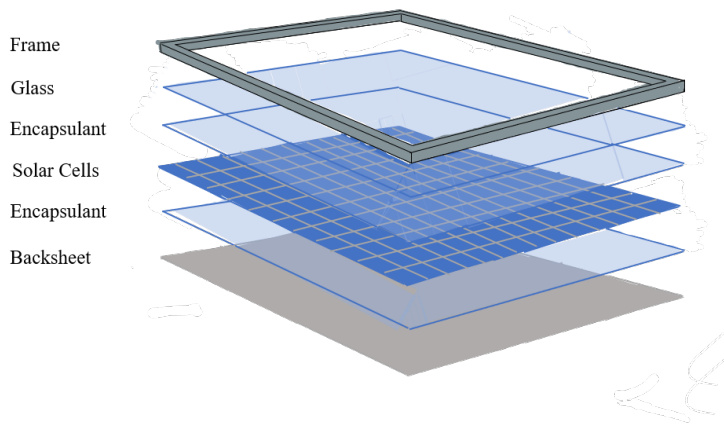
85

86 **Figure 1:** Standard silicon solar module structure.

87   Table I displays the alterations made to the solar module structure and thermal properties, along with the temperature reductions

88   experienced in the silicon layer of the solar module.

Table I: Solar module alterations along with the temperature reductions experienced

Solar Module Alteration	Temperature Reduction (°C)
Increasing Backsheet Thermal Conductivity	0.07
Decreasing Glass Thickness	0.34
Decreasing Encapsulant Thickness	0.33
Replacing Tedlar Backsheet with Glass	-0.09
Increasing Heat Transfer Coefficient of Rear Surface	16.89

It can be observed that increasing the backsheet's thermal conductivity from 0.36 W/mK to 5.5 W/mK resulted in a temperature reduction of 0.07 °C. When the thermal conductivity of the backsheet is increased further, the temperature reduction saturates to a maximum of 0.07 °C and has therefore no significant effect on the heat transfer rate. Decreasing the glass thickness from 3 mm to 2 mm resulted in a temperature reduction of 0.34° C and decreasing encapsulant thickness from 0.2 mm to 0.1 mm resulted in a temperature reduction of 0.33 °C. Both of these alterations follow a linear trend. Replacing a standard tedlar backsheet with a glass sheet resulted in an increase in temperature within the solar module of 0.09 °C and is consistent with previous studies that reported a similar increase in temperature [3, 13].

Table I shows the one alteration that resulted in a significant reduction in temperature. That is by increasing the rear surface heat transfer coefficient. The heat transfer coefficient for each surface of the solar module is determined using the Armstrong and Hurley method detailed in J.C Sánchez Barroso et al. [27]. The forced and free convective heat transfer coefficients, h_{forced} and h_{free}, are calculated using equation 1 and 2, respectively

$$h_{forced} = 8.55 \ (Wm^{-2}K^{-1}) + 2.56u \ (Wsm^{-3}K^{-1}) \tag{1}$$

$$h_{free} = \frac{Nu_{cell} \times k_{air}}{L_{cell}} \tag{2}$$

where u is the air's velocity, Nu the Nusselt number, and k_{air} the air's thermal conductivity that is equal to 0.02551 W/mK at 25°C [28]. The Nusselt number, a dimensionless number is for this case calculated as

$$Nu_{cell} = \left[0.825 + \frac{0.387 \times Ra^{1/6}}{[1+(0.492/Pr)^{9/16}]^{8/27}}\right]^2 \tag{3}$$

where Ra is the Rayleigh number and Pr is the Prandtl number. Equation (4) details how these are calculated. The Rayleigh number is a scaling parameter for driving force behind natural convection and is the ratio of buoyancy to viscous dissipation and heat diffusion [29]. The Rayleigh number is calculated with

$$Ra = Gr \times Pr = \frac{g\beta \Delta T L^3}{v^2} \times \frac{v}{k} \tag{4}$$

where Gr is the Grashof number and Pr the Prandtl number, β is the thermal expansion coefficient, g the gravitational acceleration, L the characteristic length of the system, v the kinematic viscosity and k the thermal conductivity of the fluid. The heat transfer coefficient of the front panel of the solar module is dependent on the forced and free convective heat transfer coefficients, calculated using equation 5, whereas the rear surface is made up of only the free convective heat transfer coefficient,

$$h_{front} = \sqrt[3]{h_{forced}^3 + h_{free}^3}, \quad h_{rear} = h_{free}. \tag{5}$$

The heat transfer coefficients of the front and back surfaces were found to be 8.71 W/m²K and 3.29 W/m²K, respectively. The heat transfer coefficient of the front surface is larger due to the air flow at the front of the solar module. When the heat transfer coefficient of both the front of the rear surface in the MATLAB simulation is set to 8.71 W/m²K for both surfaces, an average temperature reduction of 16.9 ºC is obtained. One of the most common and effective methods of increasing the heat transfer coefficient of a flat surface is the application of a finned heat sink. This increases the surface's area and therefore the heat transfer rate.

III. HEAT SINK MATHEMATICAL MODEL

Heat sinks are commonly used in electronic devices to aid heat dissipation. The most common heat sink configuration is a rectangular finned heat sink and the factors which affect the heat sink's ability to disperse heat are the number of fins, dictated by the fin thickness and spacing, and the fin height. A computational model of a heat sink is developed to study the heat sink heat transfer properties, using literature [30, 31]. The numerical model is solved by using MATLAB where the heat sink with a base of 0.1 m in both length and width is studied. For the purpose of the numerical model, the fluid properties are taken at 25 ºC [28] with a given temperature difference of ΔT between the ambient air of 25 ºC and the heat sink .

Primarily, the Rayleigh number, based on the length of the heat sink, is determined using equation 4. Using equation 6 one can obtain the heat sink base heat transfer coefficient, h_{base}, where a value of 0.59 is used for the constant C [31].

$$h_{base} = \frac{\left(CRa^{\frac{1}{4}}\right)k_{air}}{L} \tag{6}$$

where L is the characteristic length that refers to the base length of the heat sink. The Elenbaas correlation, EL, displayed in equation 7, determined from Elenbaas' investigations of finned heat sinks and relates to natural convective heat transfer for vertical finned heat sinks [32].

$$EL = \frac{g\beta\Delta T\, Pr\, s_{fin}^4}{Lv^2} \tag{7}$$

where s_{fin} is the distance between the fins on the heat sink. Bar-Cohen and Rohsenow further developed the Elenbaas correlations to obtain a corresponding Nusselt number correlation written in equation 8. This is rearranged to equation 9, to determine the heat transfer coefficient of the fin, h_{fin}:

$$Nu_{fin} = \frac{h_{fin}s_{fin}}{k_{air}} = \left[\frac{576}{(\eta_{fin}EL)^2} + \frac{2.873}{(\eta_{fin}EL)^{1/2}}\right]^{-1/2} \tag{8}$$

$$h_{fin} = \frac{k_{air}}{s_{fin}}\left[\frac{576}{(\eta_{fin}EL)^2} + \frac{2.873}{(\eta_{fin}EL)^{1/2}}\right]^{-1/2} \tag{9}$$

where η_{fin} corresponds to the fin efficiency. The heat transfer from the fins, Q_{fin}, is calculated using equation 10, where a constant denoted as m, is calculated using equation 11:

$$Q_{fin} = L\, k_{fin}t\, \Delta T m(\tanh(mH)) \tag{10}$$

$$m = \sqrt{\frac{h_{fin}P}{k_{fin}A_B}} \qquad (11)$$

where H is the fin height, P the fin perimeter and A_B the fin base area. The fins were modelled with a chosen material of aluminium; therefore, k_{fin} has a value of 205 W/mK [33]. The total heat sink's heat transfer, Q_T, is then calculated using equation 12, where n corresponds to the number of fins. An overall heat transfer coefficient, h_T, where T is absolute temperature, can be evaluated by equation 13:

$$Q_T = nQ_{fin} + h_{base}A_BT \qquad (12)$$

$$h_T = \frac{Q_T}{LW\Delta T} \qquad (13)$$

The developed model is used to evaluate the effects of fin thickness on the heat transfer coefficient per unit area of the base. Figure 2 displays the heat transfer coefficient per unit area of the base against the fin spacing for three different fin thicknesses: 1, 2, and 5 mm.
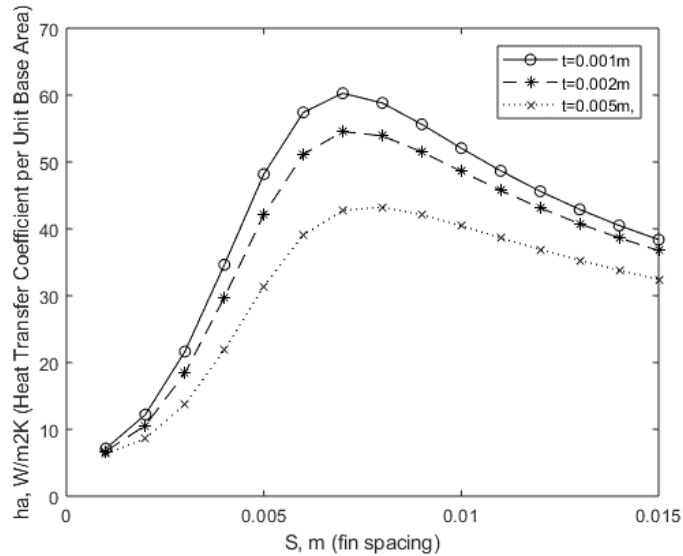
Figure 2: Heat transfer coefficient per unit base area versus fin spacing for three fin thicknesses (1mm, 2mm and 5mm)

It is observed in Figure 2 that there is an optimum fin spacing, which results in the largest heat transfer coefficient per unit area of the base value. The optimum spacing, S_{opt}, for a given heat sink can be calculated using equation 14 [31, 34]:

$$S_{opt} = 2.66 \left(\frac{Lv^2}{g\beta\eta_{fin}\,\Delta T\,Pr} \right)^{1/4} \qquad (14)$$

The optimum fin spacing is found to be at 6.745 mm and corresponds to Figure 2. The fin thickness can also be varied within the MATLAB script, and an optimum fin thickness is found at around 1 mm. However, the fin thickness optimum is not as prominent as for fin spacing.

178　　　　Varying the height of the heat sink when the thickness and optimum spacing are 0.9 mm and 6.745 mm respectively, is shown
179　　　　in Figure 3. The heat transfer coefficient per unit area of the base increases with height until a limit is reached at approximately
180　　　　0.3 m.
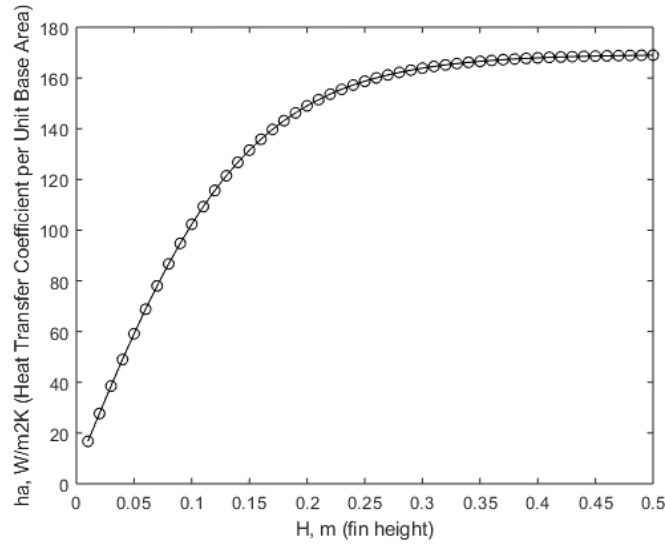
181
182
183　　**Figure 3:** Heat transfer coefficient per unit base area versus fin height

184　　　　This simulation demonstrates that although fin spacing and thickness influence the performance of a heat sink, they both reach
185　　　　a maximum before the performance decreases again. However, the simulation shows that the performance of the heat sink increases
186　　　　with fin height towards an asymptote. Thus, it was decided that the fin height would be investigated experimentally, to determine
187　　　　how this factor affects the temperature in solar modules.

188　　　　　　　　　　　　　　　　　　　IV.　　HEAT TRANSFER COEFFICIENT EXPERIMENT

189　　　　Nine heat sinks of varying heights (0.02, 0.04, 0.06, 0.08, 0.1, 0.15, 0.2, 0.25 and 0.3 m) were manufactured. While there is a
190　　　　direct correlation between thermal conductivity and material cost, aluminium is used and is a common heat sink material with a
191　　　　large thermal conductivity, low density, low weight and high strength which is affordable [35]. The heat sinks were manufactured
192　　　　from 0.9 mm thick aluminium and each of the manufactured heat sinks had a fin spacing of 10 mm. Initially, each of the heat sink's
193　　　　heat transfer coefficients were determined with the procedure developed in references [36-40]. Each of the heat sink's had a known
194　　　　heat input acting on the base of the heat sink, which is supplied using a silicone heater mat which is regulated by adjusting the
195　　　　current and voltage in an external power supply [41]. The temperature of the base of the heat sink is determined by averaging the
196　　　　temperature of three thermocouples until the point where steady state is reached. A quasi stationary steady state is assumed when
197　　　　the temperature fluctuations did not exceed 0.2 ºC. The experiment recorded the temperature of the base, the surrounding
198　　　　temperature and the power input into the heat sink.
199　　　　Fin theory is used to determine its heat transfer coefficient [42]. Initially, the constant, m, was determined using equation 11,
200　　　　allowing the heat transferred by each fin to be calculated along with the maximum heat than can be transferred from the entire heat
201　　　　sink area (equations 15 and 16). This allows the fin efficiency to be determined using equation 17.
202

203　　　$$Q_{fin} = \sqrt{h_{fin} P k_{fin} A_B} \; \Delta T \; \frac{\sinh(\mathrm{mL}) + \frac{\alpha}{k_{fin}}\cosh(mL)}{\cosh(\mathrm{mL}) + \frac{\alpha}{k_{fin}}\sinh(mL)} , \qquad (15)$$

204     $Q_{max} = h_{fin} A_{fin} \Delta T \quad ,$ (16)

205

206     $\eta_{fin} = \dfrac{Q_{fin}}{Q_{max}}.$ (17)

207

208   The weighted fin efficiency, $\eta_{weighted}$, is the efficiency of the entire heat sink. This is calculated using equation 18, where the

209   surface area of the fins, A_{fins}, is calculated along with the area of the base that does not contain fins, $A_{unfinned}$.

210

211     $\eta_{weighted} = \dfrac{\eta_{fins} A_{fins} + A_{unfinned}}{A_{total}}$ (18)

212

213   From this, the heat transfer coefficient can then be determined (equation 19). It can be noted that a heat transfer coefficient, h_{fin},

214   is needed to calculate the heat transfer coefficient. Therefore, a first guess is made as an input into the fin constant, n, and iterated

215   to determine each of the heat sinks heat transfer coefficients.

216

217     $h_{fin} = \dfrac{Q}{\eta_{weighted} A_{total} \Delta T}$ (19)

218

219   To ensure the experiment is accurate, heat rates of 10 W and 5 W are applied and by altering the heat transfer to keep a constant

220   temperature difference. The heat transfer coefficients obtained in each experiment is then averaged.

221   Figure 4 displays the heat transfer coefficient and thermal resistance of each of the heat sinks. It is observed that the heat transfer

222   coefficient reduces as the fin height increases, a potential reason for this is that the fin height restricts the air flow. This being said,

223   although the heat transfer coefficient decreases, there is a larger area so heat dissipation to the surroundings increases with height.

224   The thermal resistance measures the difficulty for each heat sink to dissipate heat to the surroundings. Again, this decreases as the

225   fin height increases, further reiterating that more heat is transferred by the heat sinks with larger fin heights.

226
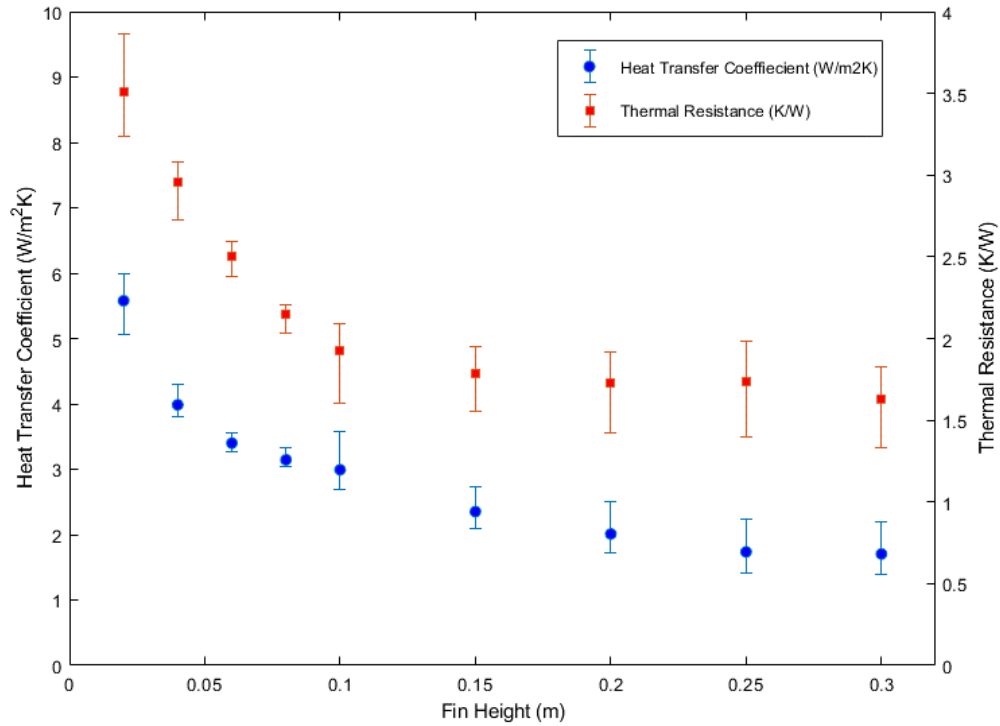
Figure 4: Heat transfer coefficient and thermal resistance varying with fin height. Error bars to indicate the experimental data range for repeat measurements.

The results follow those obtained by Wengang et al. [37], where both the heat transfer coefficient and thermal resistance decreases with increasing height. The thermal resistance illustrates the difficulty in which the heat is transferred to the surroundings from the heat sink, although this decreases, the heat transfer coefficient also decreases due to an increase in the air-flow resistance. Results obtained from Mahmoud et al. [40] studying micro-fin structures that follow the same trend, whereby an increase in height, reduces the heat transfer coefficient. A possible reason given is that the 'buoyancy-induced current' at the fin walls is competing with the lengthening downward current. Micheli et al. obtain the same trend for a micro-finned heat sink [43].

V. HEATER EXPERIMENT

To determine the temperature reduction in the solar module from each of the heat sinks a thermal experiment is carried out. This consisted of placing a solar module between the heater mat and the heat sink. The temperature is recorded between the solar module and mat and the solar module and the heat sink. Figure 5 shows a schematic diagram of the experimental set-up. A layer of thermal grease is placed between the solar module and heat sink to combat the interface losses, decreasing the risk of small air pockets being trapped in the interface, reducing heat transfer [44, 45]. For all experiments, the average room temperature was in the range 22±2°C.
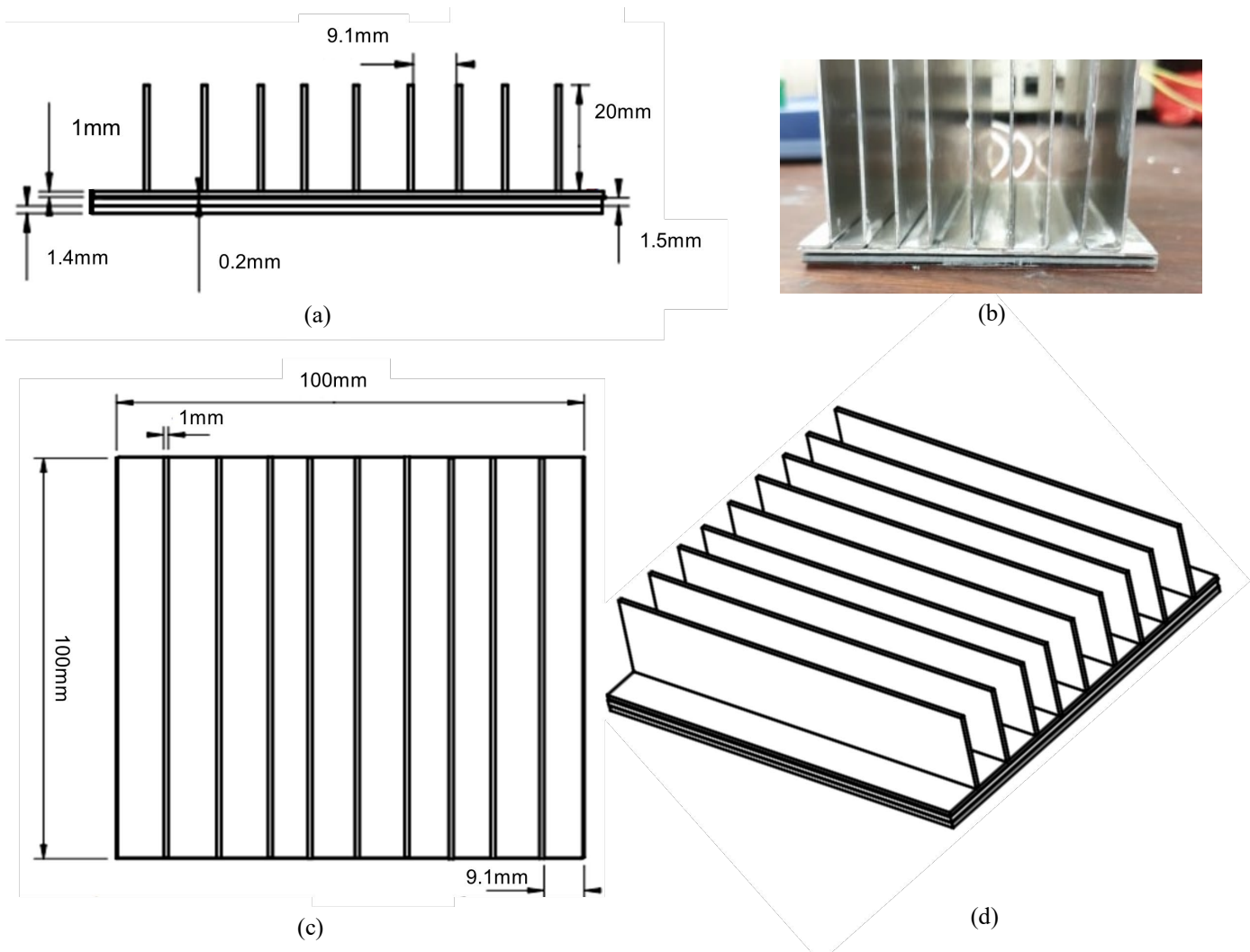
Figure 5: Illustration of thermal experimental set-up. Thermocouples were inserted into the thermal grease layer and above the heater mat. (a) Front view - from top to bottom: heat sink, thermal grease, solar module, heater mat. (b) Photograph of set-up. (c) Top view of heatsink. (d) Isometric view.

Figure 6 shows the experimental results, for the temperatures measured at the front and back of the solar module, from the thermal experiment for a power input of 10 W. Again, the temperatures are taken at steady-state conditions where the temperature fluctuations did not exceed 0.2 ⁰C.
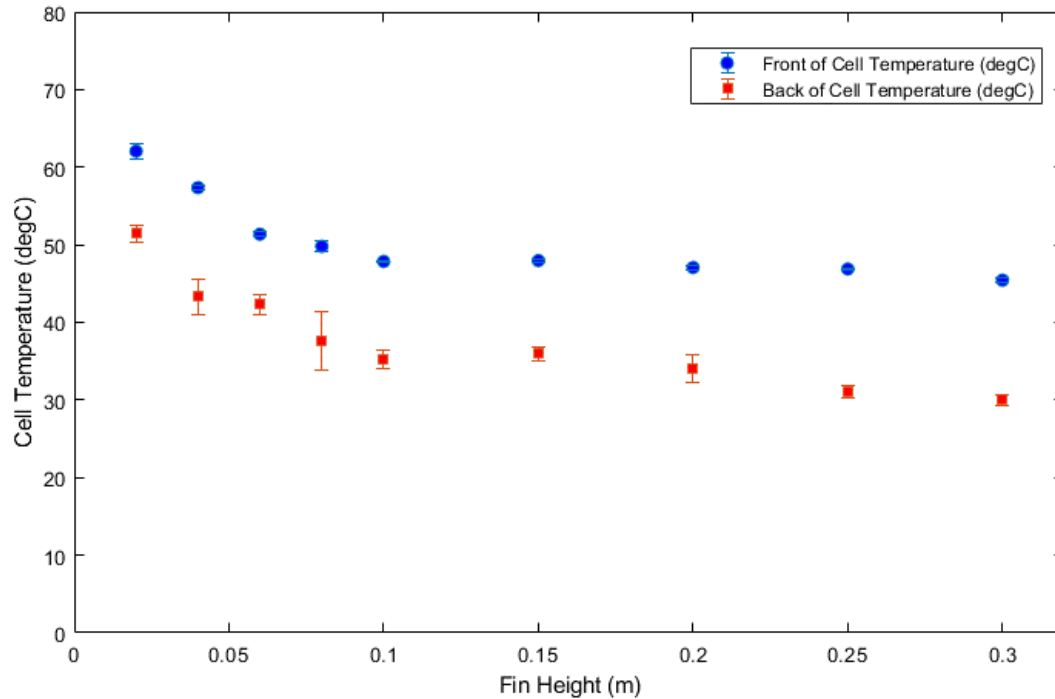
The results show that the amount of heat removed from the solar module increases with the heat sink's height. The temperature at the front of the module decreased from 62 ºC to 45.4 ºC, and the back of the module decreased from 51.5 ºC to 30 ºC. To verify that the trends obtained experimentally are accurate, theoretical approximations for the temperatures expected to be acting on the front and back surfaces of the module are determined.

A. Theoretical Approximation

Table II displays the materials, thicknesses and thermal conductivities of the layers in a standard solar module. Equation 19 was used to determine the overall thermal resistance of the system where the 'layers' relate to those the heat transfer passes after the layer of the desired temperature is reached. This was then used to determine the temperature in the solar module layers (equation 20).

Table II: Solar module architecture used in experiments and to determine theoretical approximations for the front and back module temperatures. Thermal conductivity values are taken from reference [46].

Layer	Thickness (mm)	Thermal Conductivity (W/mK)
Glass	3	0.98
EVA	0.4	0.21
Silicon Wafer	0.18	148
Tedlar	0.5	0.36

$$\frac{1}{hA} = \frac{1}{\eta_{weighted} A_{total} \alpha_{fin}} + \frac{x}{kA_{layers}} \qquad (20)$$

10

291

292     $$T_{layer} = \frac{Q}{hA} + T_{amb} \qquad\qquad\qquad\qquad (21)$$

293

294   where h is the overall heat transfer coefficient and x the layer thickness. Figures 7 and 8 display the experimental and theoretical

295   results for the temperature acting at the front and back of the solar module, respectively, with a 10 W heat rate boundary condition

296   on the front surface of the solar module.
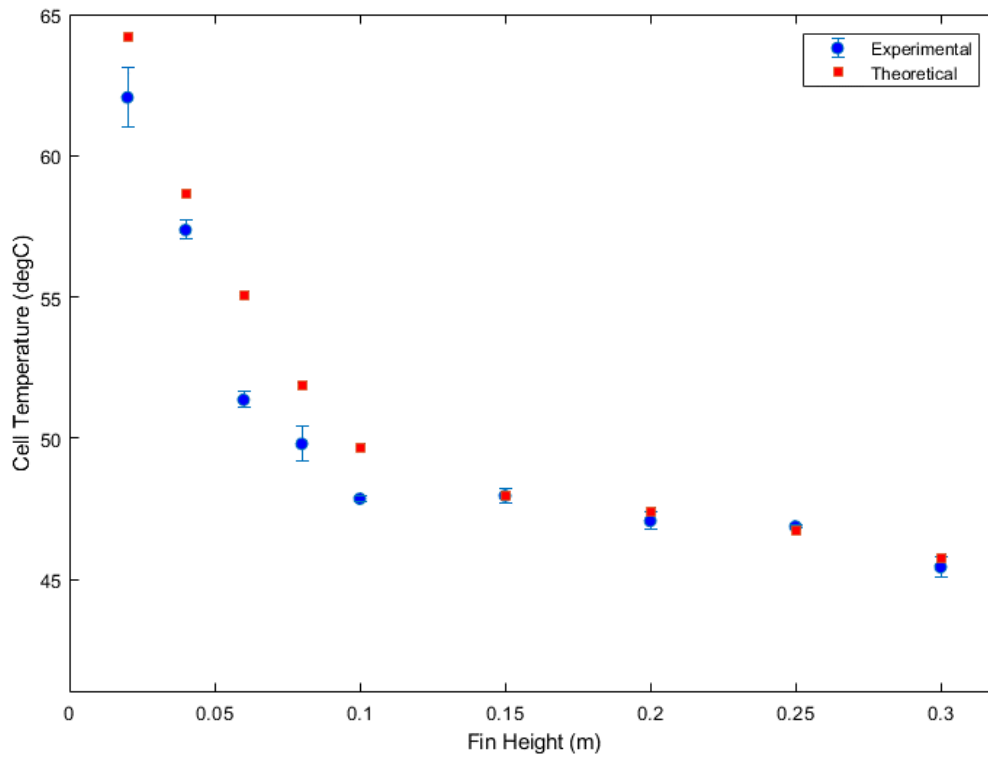
297

298   **Figure 7:** Experimental and theoretical results obtained for a heat transfer of 10 W thermal experiment for the temperature at the front of the

299   solar module. Error bars to indicate the experimental data range for repeat measurements.
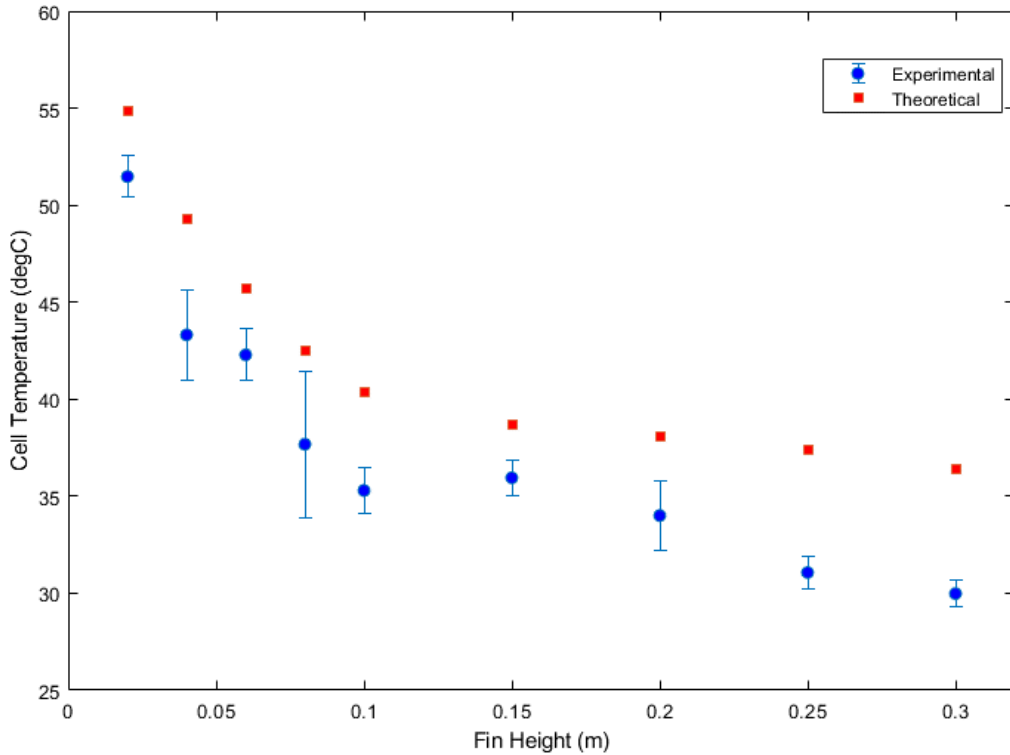
Figure 8: Experimental and theoretical results obtained for a heat transfer of 10 W thermal experiment for the temperature at the back of the solar module. Error bars to indicate the experimental data range for repeat measurements.

The results obtained experimentally follow the numerical ones closely. The largest difference between the experimental results and numerical approximations is 6.7% and 17.6% for the front and back of the solar module, respectively. The theoretical results are slightly higher than those obtained experimentally. One reason for this is that the theoretical calculation does not take into consideration the heat transferred to the surroundings from the sides of the solar module or heater mat. Also, it is assumed that the silicone heater mat is effective in supplying a constant heat transfer across its entire surface area to the solar module, which may not be the case. In addition to the experimental set-up, the numerical approximation only considers an ideal system rather all experimental uncertainties, which may also explain the differences. In any case, due to the fact that Figure 7 has theoretical values extremely close to the experimental values, it can be assumed that there is little heat lost from the sides of the silicone heater mat, resulting in a small difference between experimental and theoretical results. However, the larger difference seen in Figure 8 indicates that heat lost from the sides of the solar module is more significant, resulting in the lower experimental values, compared to those determined by the numerical approximation. One method to reduce the difference within the experiment would be to insulate the sides of the heater mat and solar module, further limiting the heat flow to one direction.

VI.   SOLAR SIMULATOR EXPERIMENT

The thermal experiment determined the effect of fin height in removing heat from a commercially available mini solar module of area 75 mm x 75 mm, and active area approximately 65 mm x 65 mm (other properties as Table II). A solar simulation experiment was carried out to find out the how the reduction in temperature affects the power output from a solar module. The

solar simulator used is an ABET Sun 2000, with a 1 kW AM1.5G lamp. The solar simulation experimental set-up is illustrated in Figure 9.
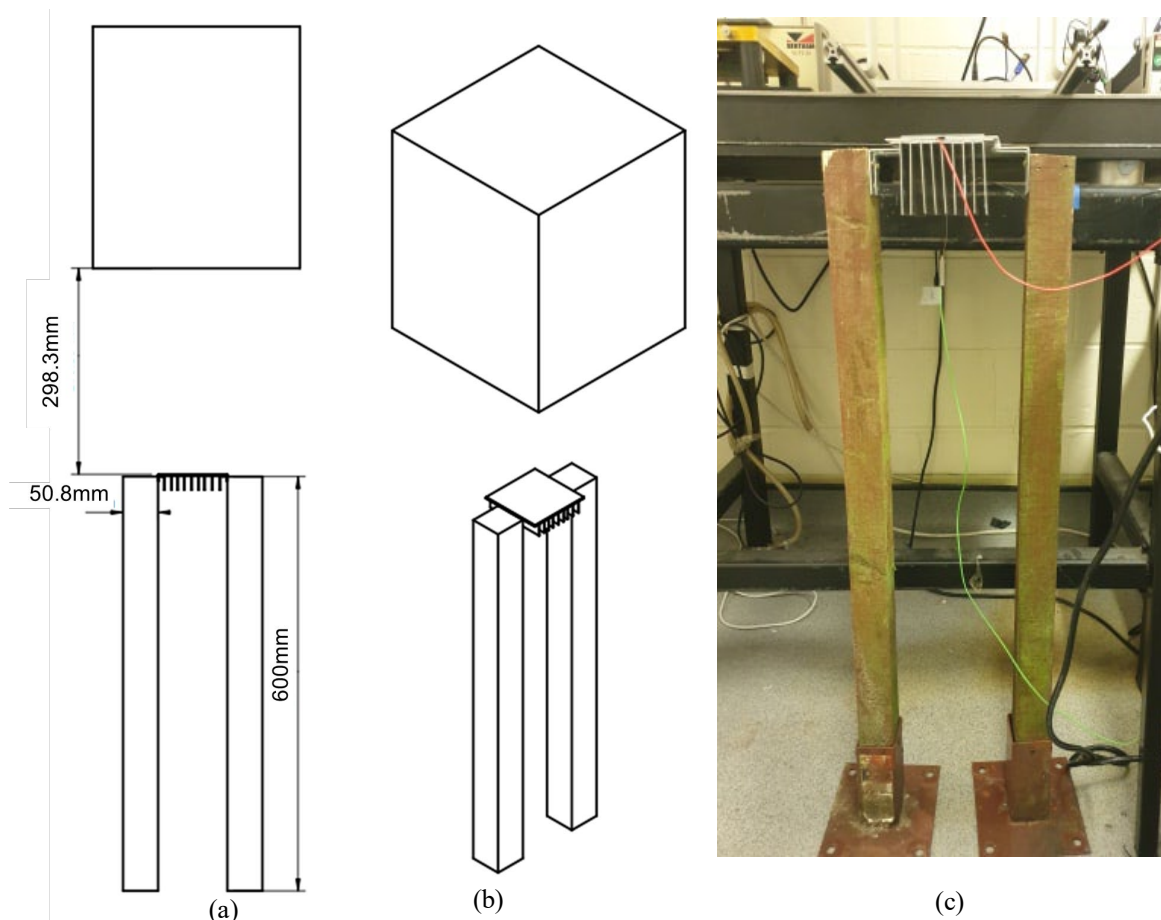
Figure 9: Solar Simulation experimental set-up showing, from top to bottom: solar simulator (represented by the cube), solar module (small, thin square), heat sink and support rig: (a) front view. (b) isometric view. (c) Photograph of set-up.

The experimental set-up consisted of a solar module with a heat sink attached to the rear surface being positioned directly under the solar simulator. The rig is designed to support the solar module and heat sink while allowing an airflow between the heat sink and the floor. Each of the heat sinks with varying fin height are tested under the solar simulator. As the different heat sinks increase in height, it is expected that the temperature of the solar module reduces. To determine the amount of energy output from the solar module in real time the current-voltage and power-voltage curve are tracked. The measuring units used is an R03-series I-V tracer.

Figure 10 displays the recorded temperature of the rear surface of the solar module as a function of fin height. The temperatures are recorded at the time when a quasi-stationary state is achieved. The data obtained followed the same trend as in the thermal experiment where, for most part, an increase in fin height results in a decrease in the rear surface temperature. The bare solar module had a rear surface temperature of 68 ⁰C and the solar module with a 300 mm heat sink attached had a rear surface temperature of 32.5 ⁰C. This is an overall reduction of 35.5 ⁰C.

The current-voltage and power-voltage curves are displayed in Figures 11 and 12, respectively. The results for the bare solar module, an aluminium base-plate, the 20 mm finned heat sink and the 100 mm finned heat sink are displayed. It is expected that a decrease in temperature will result in a slight decrease in current produced and a large increase in voltage, thus an overall increase in power is noted [7]. Figures 11 and 12 follow these trends, whereby the 20 mm finned heat sink results in a large increase in voltage and power and a further increase can be observed with the 100 mm heat sink.
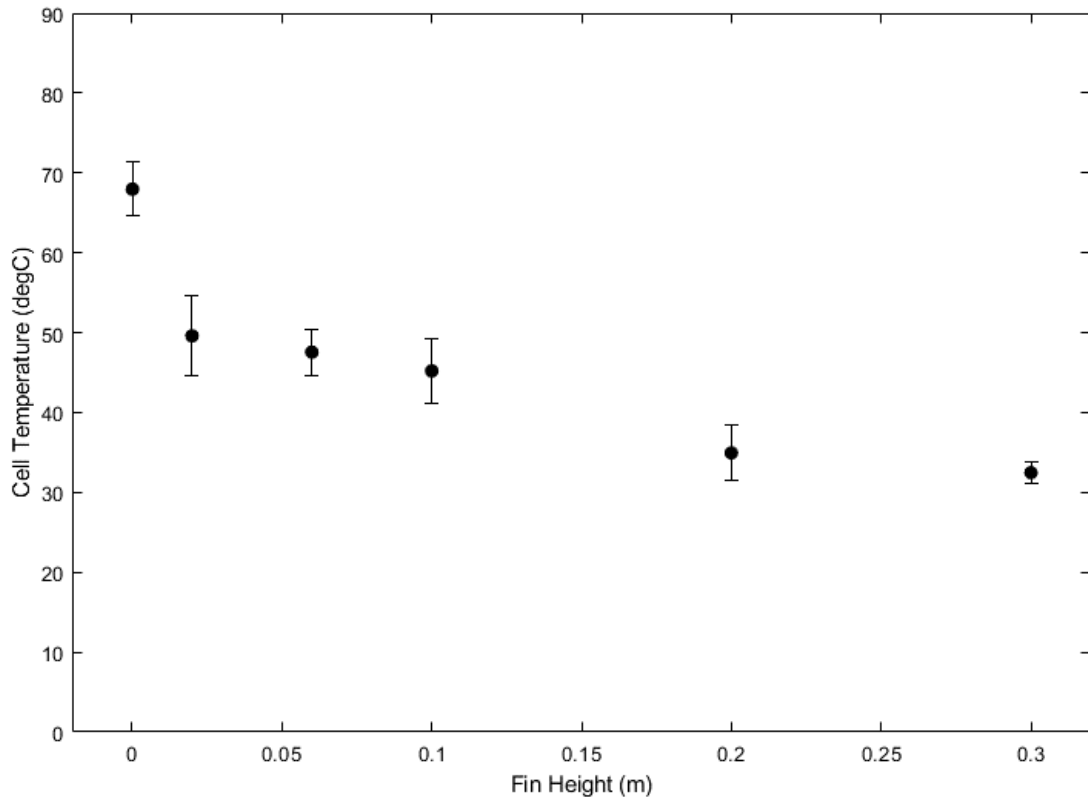
359
360 **Figure 10:** Recorded temperature at the rear surface of the solar module for varying fin heights. Error bars to indicate the experimental data
361 range for repeat measurements.

362
363

Figure 11: Current-Voltage curves for the bare solar module, the 20mm finned heat sink and the 100mm finned heat sink
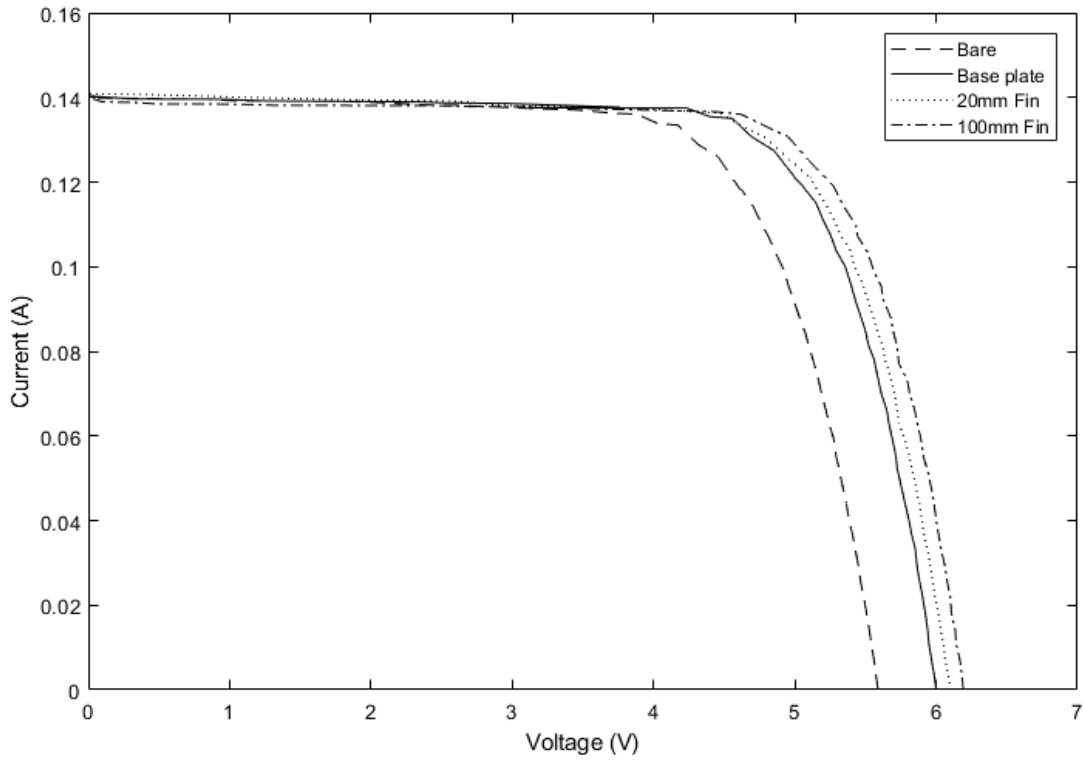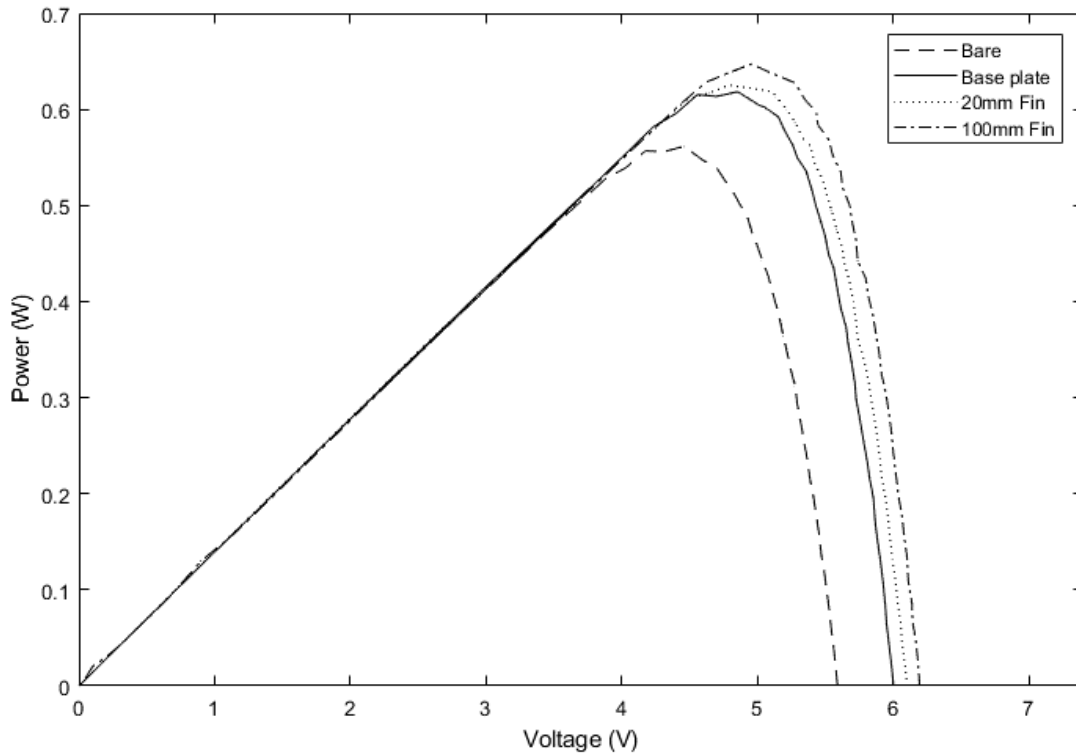
365
366 **Figure 12:** Power-Voltage curves for the bare solar module, the 20mm finned heat sink and the 100mm finned heat sink

367
368   The bare solar module has a peak power output of 0.561 W, whereas those with the base-plate, 20mm and 100mm heat sink have

369   power outputs of 0.618W, 0.625 W and 0.647 W, respectively. The base-plate alone increases the power output by 10.13%

370   compared to the power output recorded in bare solar module, whereas the 20mm finned heat sink results in an 11.34% relative

371   increase in power output. Increasing the fin height further to 100mm means the power output is further increased to 15.27%

372   compared to the bare solar module. This indicates that the addition of a finned heat sinks to a bare solar module can result in a

373   decrease of temperature, which increases the power output, as previous studies have demonstrated.

374   VII. NUMERICAL SIMULATION OF HEAT SINK INCLINATION ANGLE

375   Natural convection occurs due to buoyancy forces where hot air rises into the surroundings. The flow is caused by differences

376 in the fluid's density, generally caused by a non-isothermal fluid [47, 48]. Therefore, although the both simulations and experiments

377 indicate that the application of a heat sink to a solar module reduces the temperature, it does not give an accurate indication as to

378 what the temperature reduction will be when the solar module and heat sink combination are inclined, as if mounted on a roof. To

379 gain an understanding as to how heat sink performance depends on its orientation, a numerical simulation is carried out to

380 investigate this phenomenon.

381   In this section we investigate the heat sink's performance in correspondence to the alignment and fin height numerically. An

382 idealized model is built according to the theoretical and physical specification evaluated in Section III. To solve the model a

383 commercial finite element solver [49] is used to solve the continuity, momentum and heat equations written as

384
$$\nabla \cdot \mathbf{u} = 0 \quad (22)$$

385
$$\rho \left(\frac{\partial \mathbf{u}}{\partial t} + \mathbf{u} \nabla \cdot \mathbf{u} \right) = -\nabla p + \mu \nabla^2 \mathbf{u} + \rho \mathbf{g} \quad (23)$$

$$\rho c_p (\mathbf{u} \cdot \boldsymbol{\nabla})T = k\nabla^2 T + q \qquad (24)$$

where ρ the density, t, the time, p the pressure, μ the dynamic viscosity, $\mathbf{g}$ the gravity vector, c_p the heat capacity, T the temperature, k the thermal conductivity and q the heat flux.

The heat transfer in solids interface is used to calculate the heat flux and the local temperature within the heat sink. Boundary conditions for the system used is a constant heat rate of 10 W at the heat sink's base where the solar module is located. The choice of using 10 W is made with reference to the solar irradiance of the Earth's surface of about 1000 W/m² [50, 51]. To account for convective flow around the heat sink open far field boundaries are used having five times the heat sink's base length of 0.1 m. The heat sink is placed on the base where the is applied via a heat flux boundary condition such that the full heat rate is transported through the heat sink. On this boundary zero, the heat transfer in fluids interface is used to calculate convection where density changes of the surrounding air are imposed by the heat flux through the heat sink. No-slip velocity boundary conditions are applied to all boundaries. To calculate for pressure a zero-point constraint is applied at the adiabatic boundary. To study the degree of alignment range of a solar module, the gravity vector is alternated by alignment angle, γ, where $\gamma = 90°$ and $180°$ are the heat sinks fins facing in the horizontal and the vertical direction, respectively. All configurations are studied with the same initial conditions of a stagnant fluid with a uniformly distributed room temperature of 20 °C. While the main heat is transported by convection, we have neglected surface to ambient radiation in this study. A triangular mesh is created with 650,000 elements where 14,700 are in the solid domain. This mesh independence test showed reliable solutions for about 500,000 elements. The numerical model solved the continuity, momentum and heat equations with a time dependent solver. Results are post-processed after an equilibration process of about 20 min where the heat flow and temperature had settled to a quasi-stationary state.

We now present the results of the computational model in terms of surface temperature for a fin height of 120 mm at four different alignment angles, γ, in Figure 13. The temperature distribution shows a dependence of heat transport over the fins at different γ indicating an enhanced heat transport by natural convection. The highest performance of the heat sink is obtained at $\gamma = 90°$ where thermal diffusion and viscous dissipation provide the best heat transport over the fins. Increasing γ up to $180°$ reduces the heat transport by natural convection as the flow direction is unable to dissipate away from the fins. Thus, a higher surface temperature is seen.

$\gamma = 90°$ $\gamma = 120°$ $\gamma = 150°$ $\gamma = 180°$
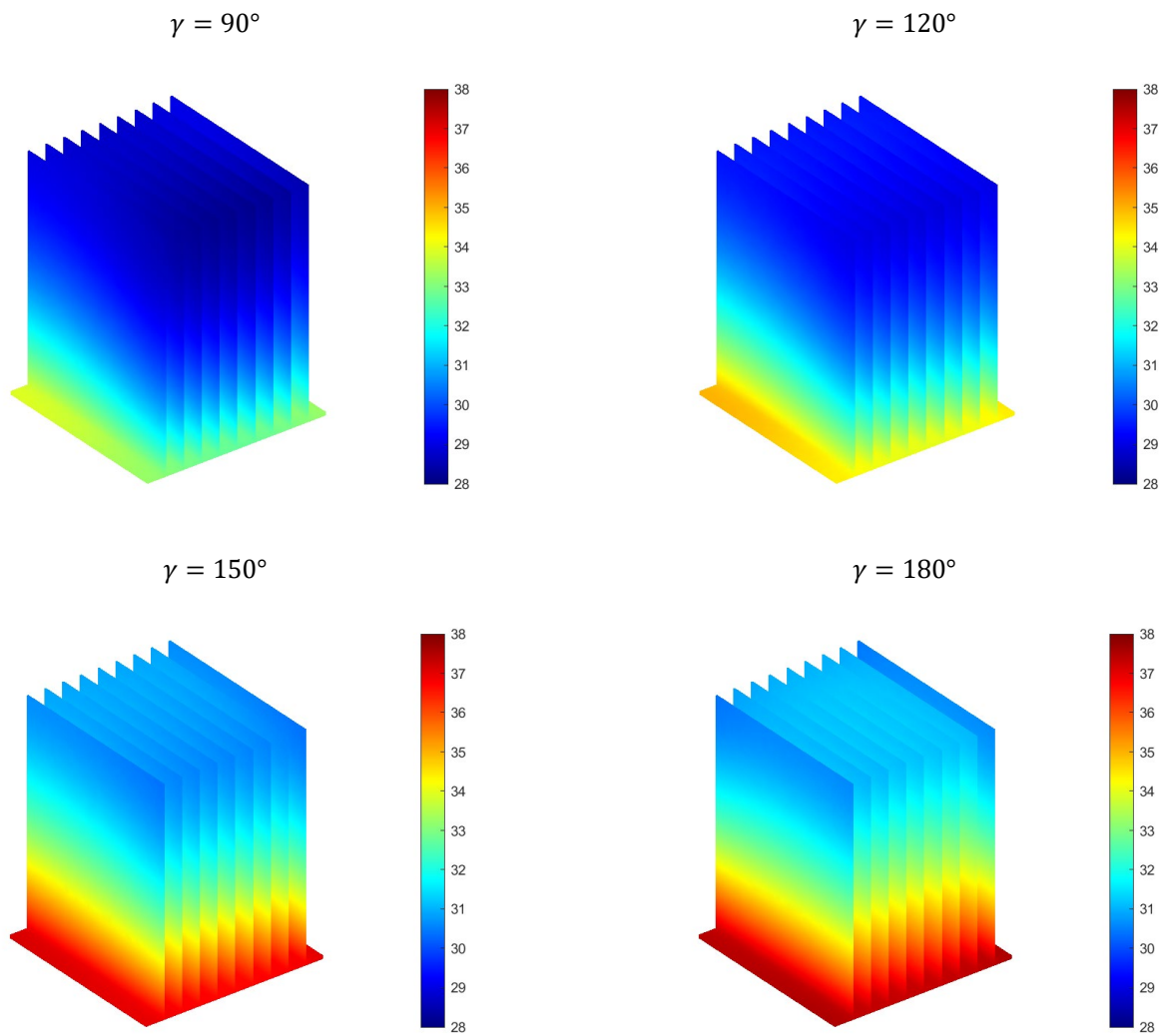
Figure 13: Surface temperature (°C) of heat sink at different alignment angles, γ, for a given fin height of 120 mm.

While the fin height may play an additional factor to the heat sink's heat transport ability, a parametric study is carried out for various inclination angles and fin heights. Figure 14 shows the surface temperature for the case of $\gamma = 90°$ with different fin heights ranging from 20 mm to 180 mm. The results indicate a significant reduction in temperature when the fin height increases. As such the increase in the heat sink's surface area is crucial for a larger heat flow to reduce the overall temperature of the system that is seen in Figure 14 when fin height is increased.

418

$H = 20$ mm

$H = 80$ mm

$H = 150$ mm

$H = 180$ mm
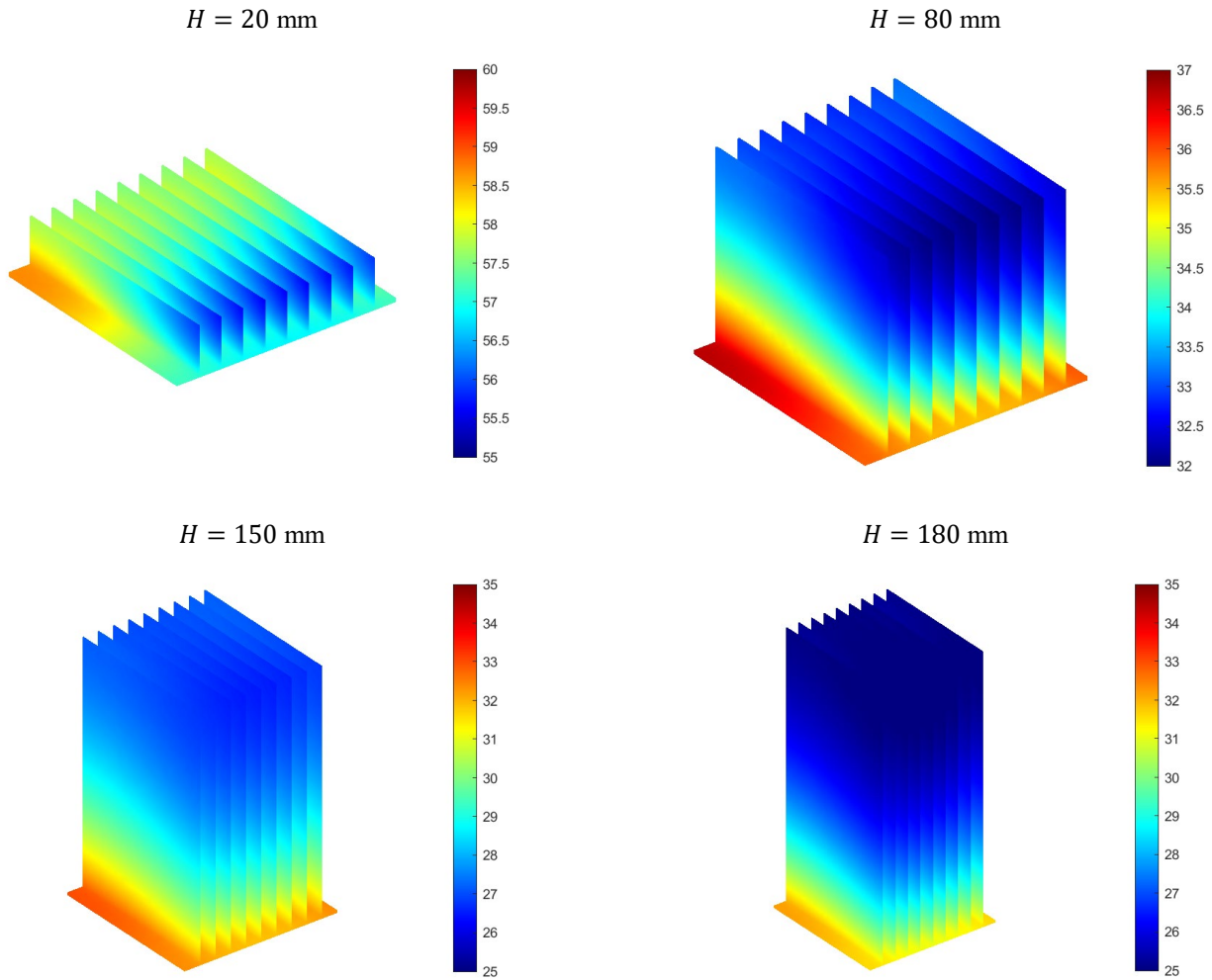
419 **Figure 14:** Surface temperature (°C) of heat sink at different fin height, H, for a given alignment angle of $\gamma = 90°$.

420 An overview of the investigated parameter range is given in Figure 15 showing the volumetric averaged heat sink's temperature.
421 The averaged volumetric temperature of each time dependent study is taken after an equilibration time where the system had
422 reached a quasi-stationary steady state condition. For the complete set, results are evaluated after 20 min which is far above the
423 temperature equilibration of the system. This provided a comparison between different inclination angles and fin heights.
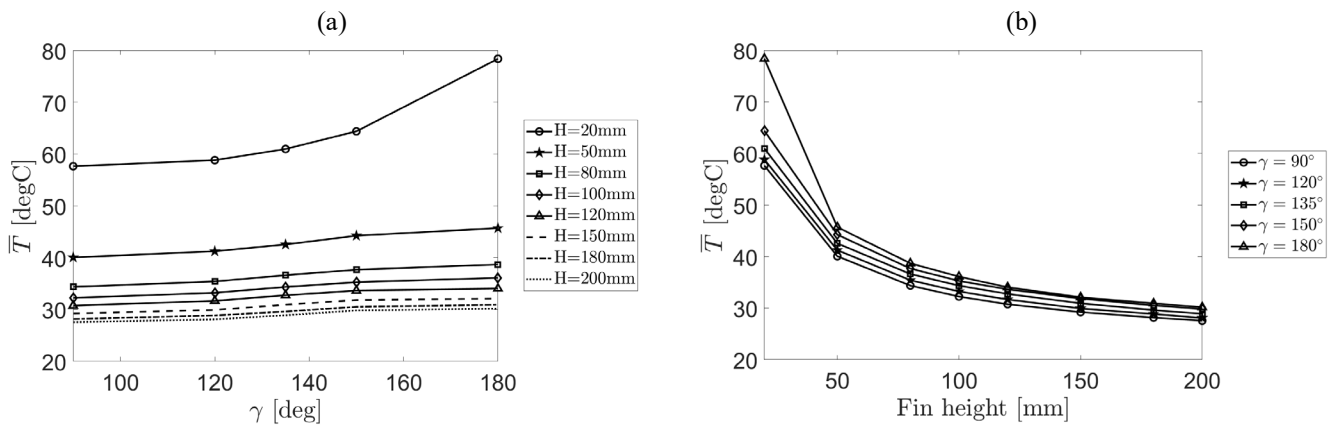
424 **Figure 15:** Average heat sink temperature at different inclination angles, γ, in (a) and different fin height in (b).

The reveal a power dependence of the fin height and average temperature that may be expressed for several inclination angles see Table III.

Table III: Inclination angle with the corresponding power dependence.

Inclination angle, γ	Power Law
90	$143.43T^{-0.318}$
120	$147.13\,T^{-0.318}$
135	$153.84\,T^{-0.321}$
150	$166.82\,T^{-0.332}$
180	$242.67\,T^{-0.404}$

The numerical results demonstrate that heat sink orientation is a factor in its performance especially for heat sinks with shorter fins. However, it can be observed as the fin height increases the orientation has a less significant effect on heat sinks performance. This is an important consideration when choosing the most suitable fin height to cool solar modules.

VIII.CONCLUSION

This study investigated the reduction of temperature within a silicon solar module. For this purpose, finned heat sinks with different fin heights and inclination angle have been investigated to reduce temperature and increase power output. Results suggest there is an overall benefit of applying a heat sink to a solar module under laboratory conditions. However, further studies need to be carried out to study the advantages in a realistic application area.

To summarise, the addition of a heat sink to the rear surface of a solar module reduces the module's operating temperature. The thermal experiment determined that increasing a heat sink's fin height increases its performance in removing heat from the solar module, until a limit is reached at about 0.2 m.

The numerical simulation showed that a heat sink's performance is not only dependent on the fin height but also on its orientation, where convective heat transport through the fins plays an important role when considering certain alignment angles. The numerical simulation can also be further developed to study the effects of fluid flow over the heat sink. This will give an indication of solar module temperature reduction expected in a realistic environment.

The experiments with the solar simulator revealed corresponding results to the numerical simulations in terms of the benefits with respect to temperature reduction. Further experiments obtained an increased power production when a heat sink is applied to the back of a solar module. Output were higher by 11.34% and 15.27% for a 20mm and 100mm fin height, respectively, compared to the bare solar module.

These findings indicate that implementing heat sinks to the back of silicon solar modules to reduce temperature could be beneficial. To determine whether the application of heat sinks to the rear surface of solar modules is a viable solution in full-scale modules would depend on the relative benefits of implementation, both in terms of cost-benefit analysis, the ease of incorporation and their reliability. The 20mm heat sink brought module efficiency improvements 11.34% (relative) higher than the bare solar module. Assuming an equivalent increase is possible in a full-scale module, would imply 11% more energy could be generated by a module over its operational lifetime. This might feasibly outweigh additional costs and challenges generated by the integration of heat sink technology. An accurate determination of this is outside the scope of this current study. One further advantage to using a heat sink to moderate temperature is the knock-on benefit with regards to a reduction in solar module degradation. Although the heat sink-induced increase in power output is relatively small, the greatest appeal of the addition of a heat sink to a solar module might be the potential to increase module lifetime.

REFERENCES

[1]   S. Murmson. "The Average Photovoltaic System Efficiency." https://sciencing.com/average-photovoltaic-system-efficiency-7092.html (accessed 18, Nov, 2018, 2018).

[2]   J. N. Roy, G. R. Gariki, and V. Nagalakhsmi, "Reference module selection criteria for accurate testing of photovoltaic (PV) panels," *Solar Energy,* vol. 84, no. 1, 2010, doi: 10.1016/J.SOLENER.2009.09.007.

[3]   J. Oh *et al.*, "Reduction of PV Module Temperature Using Thermally Conductive Backsheets," *IEEE Journal of Photovoltaics,* vol. 8, no. 5, pp. 1160-1167, Aug 2018, doi: 10.1109/JPHOTOV.2018.2841511.

[4]   F. Ghani, G. Rosengarten, M. Duke, and J. K. Carson, "On the influence of temperature on crystalline silicon solar cell characterisation parameters," *Solar Energy,* vol. 112, pp. 437-445, 2015, doi: 10.1016/j.solener.2014.12.018.

[5]   V. Jafari Fesharaki, Majid Dehghani, and J. Jafari Fesharaki, "The Effect of Temperature on Photovoltaic Cell Efficiency," in *Proceedings of the 1st Interna*

[6]   A. Javed, "The Effect of Temperature on the Silicon Solar Cell," *International Journal of Emerging Technologies in Computational and Applied Sciences,* pp. 305-308, 2014.

[7]   A. R. Amelia, Y. M. Irwan, W. Z Leow, M. Irwanto, I. Safwati, and M. Zhafarina, "Investigation of the Effect Temperature on Photovoltaic (PV) Panel Output Performance," *Advances Science Engineering Information Technology,* vol. 6, no. 5, pp. 682-688, 2016.

[8]   M. Benghanem, A. A. Al-Mashraqi, and K. O. Daffallah, "Performance of solar cells using thermoelectric module in hot sites," *Renewable Energy,* vol. 89, pp. 51-59, 2016, doi: 10.1016/j.renene.2015.12.011.

[9]   D. Polverini, M. Field, E. Dunlop, and W. Zaaiman, "Polycrystalline silicon PV modules performance and degradation over 20 years," *Progress in Photovoltaics: Research and Applications,* vol. 21, no. 5, pp. 1004-1015, 2013, doi: 10.1002/pip.2197.

[10]   PVeducation. "PV Module Temperature." https://www.pveducation.org/pvcdrom/modules-and-arrays/pv-module-temperature (accessed 25, March, 2019).

[11]   Yeom, K. M., Kim, S. U., Woo, M. Y., Noh, J. H., Im, S. H., Recent Progress in Metal Halide Perovskite-Based Tandem Solar Cells. Adv. Mater. 2020, 32, 2002228. https://doi.org/10.1002/adma.202002228.

[12]   T. J. Silverman, I. Subedi, N. J. Podraza, I. M. Slauch, and V. E. Ferry, "Reducing Operating Temperature in Photovoltaic Modules," *IEEE Journal of Photovoltaics,* vol. 8, no. 2, pp. 532-540, Feb 2018, doi: 10.1109/JPHOTOV.2017.2779842.

[13]   J. P. Singh, I. M. Siyu Guo, A. G. Peters, T. M. Aberle, and T. M. Walsh, "Comparison of Glass/Glass and Glass/Backsheet PV Modules Using Bifacial Silicon Solar Cells," *Photovoltaics, IEEE Journal of,* vol. 5, no. 3, pp. 783-791, 2015, doi: 10.1109/JPHOTOV.2015.2405756.

[14]   G. Colţ, "Performance evaluation of a PV panel by rear surface water active cooling," in *2016 International Conference on Applied and Theoretical Electricity (ICATE),* 6-8 Oct. 2016 2016, pp. 1-5, doi: 10.1109/ICATE.2016.7754634.

[15]   H. Bahaidarah, A. Subhan, P. Gandhidasan, and S. Rehman, "Performance evaluation of a PV (photovoltaic) module by back surface water cooling for hot climatic conditions," *Energy,* vol. 59, pp. 445-453, 2013, doi: 10.1016/j.energy.2013.07.050.

[16]   Y. M. Irwan *et al.*, "Analysis Air Cooling Mechanism for Photovoltaic Panel by Solar Simulator," *International Journal of Electrical and Computer Engineering,* vol. 5, no. 4, pp. 636-643, 2015.

[17]   A. Tiwari, M. S. Sodha, A. Chandra, and J. C. Joshi, "Performance evaluation of photovoltaic thermal solar air collector for composite climate of India," *Solar Energy Materials and Solar Cells,* vol. 90, no. 2, pp. 175-189, 2006, doi: 10.1016/j.solmat.2005.03.002.

[18]   A. Q. Jakhrani, A. R. Jatoi, and S. H. Jakhrani, "Analysis and Fabrication of an Active Cooling System for Reducing Photovoltaic Module Temperature," *Engineering,* vol. 7, no. 5, pp. 1980-1986, 2017, doi: 10.5281/zenodo.1037205.

[19]   A. H. Alami, "Synthetic clay as an alternative backing material for passive temperature control of photovoltaic cells," *Energy,* vol. 108, no. C, pp. 195-200, Aug 2016, doi: 10.1016/j.energy.2015.05.029.

[20]   E. Cuce, T. Bali, and S. A. Sekucoglu, "Effects of passive cooling on performance of silicon photovoltaic cells," *International Journal of Low-Carbon Technologies,* vol. 6, no. 4, pp. 299-308, Sept 2011, doi: 10.1093/ijlct/ctr018.

[21]   R. Stropnik and U. Stritih, "Increasing the efficiency of PV panel with the use of PCM," *Renewable Energy,* vol. 97, pp. 671-679, 2016, doi: 10.1016/j.renene.2016.06.011.

[22]   M. J. Huang, P. C. Eames, B. Norton, and N. J. Hewitt, "Natural convection in an internally finned phase change material heat sink for the thermal management of photovoltaics," *Solar Energy Materials and Solar Cells,* vol. 95, no. 7, pp. 1598-1603, 2011, doi: 10.1016/j.solmat.2011.01.008.

[23]   A. A. Amr, A. A. M. Hassan, M. Abdel-salam, and A. H. M. El-Sayed, "Enhancement of photovoltaic system performance via passive cooling," in *2017 Nineteenth International Middle East Power Systems Conference (MEPCON)*, 19-21 Dec. 2017 2017, pp. 1430-1439, doi: 10.1109/MEPCON.2017.8301371.

[24]   S. K. Natarajan, T. K. Mallick, M. Katz, and S. Weingaertner, "Numerical investigations of solar cell temperature for photovoltaic concentrator system with and without passive cooling arrangements," *International Journal of Thermal Sciences,* vol. 50, no. 12, pp. 2514-2521, 2011, doi: 10.1016/j.ijthermalsci.2011.06.014.

[25]   H. Xu *et al.*, "Coupled natural convection and radiation heat transfer of hybrid solar energy conversion system," *International Journal of Heat and Mass Transfer,* vol. 107, pp. 468-483, 2017, doi: 10.1016.

[26]   J. Allan, H. Pinder, and Z. Dehouche, "Enhancing the thermal conductivity of ethylene-vinyl acetate (EVA) in a photovoltaic thermal collector," *AIP Advances,* vol. 6, no. 3, pp. 035011-035011-9, Mar 2016, doi: 10.1063/1.4944557.

[27]   J. C. Sánchez Barroso, N. Barth, J. P. M. Correia, S. Ahzi, and M. A. Khaleel, "A computational analysis of coupled thermal and electrical behavior of PV panels," *Solar Energy Materials and Solar Cells,* vol. 148, pp. 73-86, April 2016, doi: 10.1016/j.solmat.2015.09.004.

[28]   Keenan, Chao, and Keyes, "Properties of Air," P. T. a. Charts, Ed., ed.

[29]   Nuclear Power. "What is Rayleigh Number." https://www.nuclear-power.net/nuclear-engineering/heat-transfer/introduction-to-heat-transfer/characteristic-numbers/what-is-rayleigh-number/ (accessed 13, Nov, 2018).

[30]   A. Bar-Cohen and W. M. Rohsenow, "Thermally Optimum Spacing of Vertical, Natural Convection Cooled, Parallel Plates," *Journal of Heat Transfer,* vol. 106, no. 1, pp. 116-123, 1984.

[31]   A. Bar-Cohen, M. Iyengar, and A. D. Kraus, "Design of Optimum Plate-Fin Natural Convective Heat Sinks," vol. 125, pp. 208-216, 2003, doi: 10.1115/1.1568361.

[32]   M. Ahmadi, G. Mostafavi, and M. Bahrami, "Natural convection from rectangular interrupted fins," *International Journal of Thermal Sciences,* vol. 82, no. 1, pp. 62-71, 2014, doi: 10.1016/j.ijthermalsci.2014.03.016.

[33]   G. S. U.-. Hyperphysics. "Thermal Conductivity;." http://hyperphysics.phy-astr.gsu.edu/hbase/Tables/thrcn.html (accessed 10, Oct, 2018).

[34]   R. E. Simons. "Estimating Natural Convection Heat Transfer for Arrays of Vertical Parallel Flat Plates." https://www.electronics-cooling.com/2002/02/estimating-natural-convection-heat-transfer-for-arrays-of-vertical-parallel-flat-plates/ (accessed 1, Nov, 2018).

[35]   Radian. "Aluminium Heatsink." https://www.radianheatsinks.com/aluminum-heatsink/ (accessed 28, Oct, 2018).

[36]   S. Hireholi, K. S. Shashishekhar, and S. G. Milton, "EXPERIMENTAL DETERMINATION OF HEAT TRANSFER COEFFICIENT BY NATURAL CONVECTION FOR A COMMERCIALLY AVAILABLE HEAT SINK USED FOR COOLING OF ELECTRONIC CHIPS," *International Journal of Mechanical and Industrial Engineering (IJMIE),* vol. 3, no. 1, 2013.

[37] H. Wengang, W. Lulu, Z. Zongmin, L. Yanhua, and L. Mingxin, "Research on simulation and experimental of thermal performance of LED array heat sink," *10th International Symposium on Heating, Ventilation and Air Conditioning, ISHVAC2017,* vol. 205, pp. 2084-2091, 2017, doi: 10.1016/j.proeng.2017.10.102.

[38] S. Hireholi, K. S. Shashishekhar, and G. S. Milton, "Experimental and Theoretical Study of Heat Transfer by Natural Convection of a Heat Sink Used for Cooling of Electronic Chip," *International Journal of Engineering Invenions,* vol. 2, no. 2, 2013.

[39] S. N. Shehab, "Experimental Study of Free-Convection from Rectangular Fins Array on a Heated Horizontal Plate with Notch Effects," *Al-Nahrain Journal for Engineering Sciences (NJES),* vol. 20, no. 1, pp. 140-148, 2017.

[40] S. Mahmoud, R. Al-Dadah, D. K. Aspinwall, S. L. Soo, and H. Hemida, "Effect of fin geometry on natural convection heat transfer of horizontal microstructures," *Applied Thermal Engineering,* vol. 31, pp. 627-633, 2011, doi: 10.1016/j.applthermaleng.2010.09.017.

[41] RS Components. "Silicone Heater Mat, 10W, 100x100mm, 12V dc." https://uk.rs-online.com/web/p/silicone-heater-mats/0245540/ (accessed 20, Jan, 2019).

[42]   Dr Stephen Houston, "Thermodynamics 2 - Lecture Notes," Heriot-Watt University, 2019.

[43] L. Micheli, K. S. Reddy, and T. K. Mallick, "General correlations amount geometry, orientation and thermal performance of natural convective micro-finned heat sinks," *International Journal of Heat and Mass Transfer,* vol. 91, pp. 711-724, 2015, doi: 10.1016/j.ijheatmasstransfer.2015.08.015.

[44] Radian. "What is a heatsink?" https://www.radianheatsinks.com/heatsink/ (accessed 22, Oct, 2018).

[45] RS Components. "Silicone Thermal Grease, 5W/mK." https://uk.rs-online.com/web/p/thermal-grease/7074736/ (accessed 18, nov, 2018).

[46] B. Lee, J. Z. Lui, B. Sun, C. Y. Shen, and G.C.Dai, "Thermally conductive and electrically insulating EVA composite encapsulants for solar photovoltaic (PV) cell," *eXPRESS Polymer Letters,* vol. 2, no. 5, pp. 357-363, 2008, doi: DOI: 10.3144/expresspolymlett.2008.42.

[47] Wakefield-vette. "Natural Convection Overview." http://www.wakefield-vette.com/products/natural-convection.aspx (accessed 23, March, 2019).

[48] N. S. Gibanov and M. A. Sheremet, "Effect of the buoyancy force on natural convection in a cubical cavity with a heat source of triagular cross-section," *Materials Science and Engineering,* vol. 124, 2016, doi: doi:10.1088/1757-899X/124/1/012057.

[49] COMSOL Multiphysics v5.4 (2018) https://uk.comsol.com/ (accessed 5, Mar, 2019).

[50] Columbia University Press, "Solar Radiation," pp. 2.1-2.4, 1994.

[51] J. D. Solar. "Solar Radiation." http://ecgllp.com/files/3514/0200/1304/2-Solar-Radiation.pdf (accessed 1, April, 2019).